

# **An Electron Model of an FFAG Muon Accelerator**

**E. Keil and A.M. Sessler\***

## **Abstract**

Parameters are derived and exhibited for the lattice and RF system of an electron model (10-20 MeV) of a non-scaling FFAG ring for accelerating muons. Spacings, magnet types and dimensions, and number of cells are presented. The model circumference is 10 meters, and the magnet apertures are 12 mm  $\times$  20 mm. The parameters of the magnetic components are compared to those of existing magnets. The tune variation with momentum is similar to that in a full machine and would allow the study of resonance crossing. The consequences of misaligned magnets are studied by simulation. The variation of orbit length with momentum is less than 35 mm and would allow the study of acceleration outside a bucket. A 100 mm straight section, in each of 33 cells, is adequately long for an RF cavity operating at 3 GHz. The accelerating voltage needed is calculated. Practical RF system design issues, e.g. RF power, and the limit on the bunch population due to beam loading are estimated.

Geneva, Switzerland

December 10, 2003

---

\*Lawrence Berkeley National Laboratory, Berkeley CA, USA

# 1 Introduction

This brief note discusses an electron model for a non-scaling FFAG ring accelerating muons. The lattice parameters are close to those circulated by J.S. Berg [1] at the FFAG Workshop, held from 13 to 17 October 2003 at BNL. This model has about 10 m circumference, and accelerates electrons from 10 to 20 MeV. The lattice consists of 33 periods, each 0.3 m long. Focusing is by a triplet of combined-function dipoles. Each period includes a straight section of 0.1 m length, which is long enough to house an RF cavity that operates at about 3 GHz and is half an RF wavelength long. The accelerating voltage needed is calculated. Practical RF system design issues, e.g. RF power, and the limit on the bunch population due to beam loading are estimated.

Table 1: Parameters of the electron model lattice at the reference energy 15 MeV

Magnet style	Sector	Rectangular	
File	nov03c	nov03e	
Number of cells	33	33	
Cell length	0.3	0.3	m
F magnet length	30	30	mm
F magnet angle	-73.181	-72.551	mrاد
F magnet gradient	12.364	12.940	T/m
F magnet field	-121.982	-120.932	mT
D magnet length	100	100	mm
D magnet angle	336.762	335.502	mrاد
D magnet gradient	-6.849	-6.445	T/m
D magnet field	168.400	167.770	mT

# 2 Electron Model Lattice Parameters

Tab. 1 shows the main parameters of the electron model lattice. Two horizontally focusing gradient dipoles surround a horizontally defocusing gradient dipole. The distance between the dipoles in the triplet is 20 mm. Two styles of combined-function dipoles are considered, sector magnets and rectangular magnets. The reference trajectory enters and leaves sector magnets at right angles. Rectangular magnets have parallel end faces, and the reference trajectory enters and leaves them at an angle. Fig. 1 shows the optical functions  $\sqrt{\beta_x}$ ,  $\sqrt{\beta_y}$ , and dispersion  $D_x$

for sector magnets. The RF cavity is at the maximum of  $D_x$ . Hence, it is possible that dangerous synchro-betatron resonances are excited.

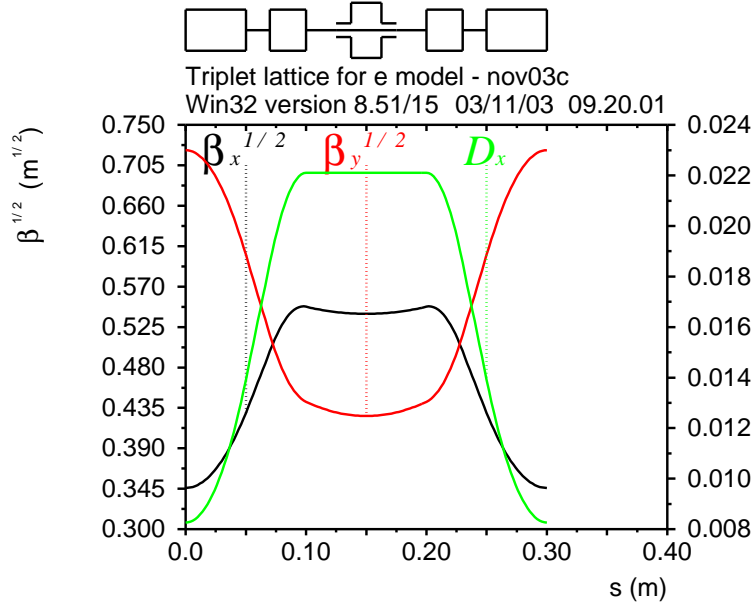


Figure 1: Orbit functions in a cell with sector dipoles. The abscissa starts and ends at the centre of the D dipole.

The gradients of the F and D dipoles are adjusted such that the phases advance by  $q_x = 0.233$  and  $q_y = 0.184$  in a lattice cell on the reference orbit at  $\delta p/p = 0$ . Here and in the following, we use  $q_x$  and  $q_y$  for the tunes of single cells, and  $Q_x$  and  $Q_y$  for the tunes in the whole ring. With these nominal tunes, the tunes  $q_x$  and  $q_y$  at the lower edge of the momentum range should remain well below the systematic half-integral stop band at  $q = 1/2$ . The bending angles in the F and D magnets are adjusted such that the flight time through a lattice cell is approximately independent of the relative momentum error to first order near  $\delta p/p = 0$ . All results are computed with MAD [2] although its correctness for relative momentum errors much larger than a few percent is questionable.

The optical functions with rectangular magnets are indistinguishable from those shown in in Fig. 1. However, Tab. 1 shows that the D magnet gradient changes by about 6%, more than the other parameters, when the magnet style changes.

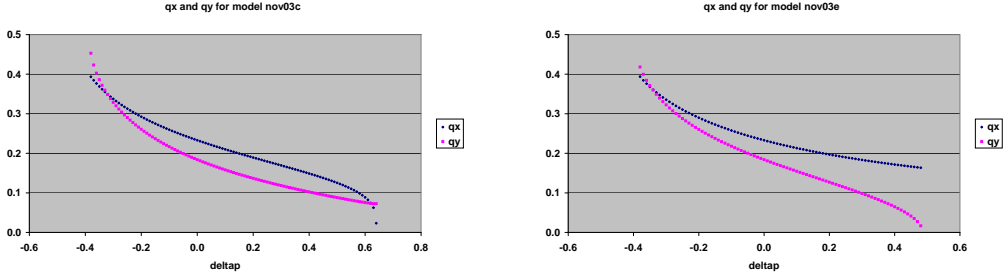


Figure 2: Variation of the tunes  $q_x$  and  $q_y$  in a cell with the relative momentum error  $\delta p/p$ , for sector dipoles on the left, for rectangular dipoles on the right.

## 2.1 Momentum Range

Fig. 2 shows the variation of the tunes  $q_x$  and  $q_y$  with the momentum error  $\delta p/p$  for a single lattice cell. In both magnet styles, the lower edge of the momentum range is caused by the vertical tune  $q_y$  approaching  $1/2$  from below. The upper edge of the momentum range is caused by the horizontal tune  $q_x$  approaching 0 from above in sector magnets, and by the vertical tune  $q_y$  approaching 0 from above in rectangular magnets. The betatron oscillations are stable within the momentum range  $-0.38 \leq \delta p/p \leq 0.64$  in the lattice with sector magnets, and within the range  $-0.38 \leq \delta p/p \leq 0.48$  in the lattice with rectangular magnets. The former range is larger than the latter.

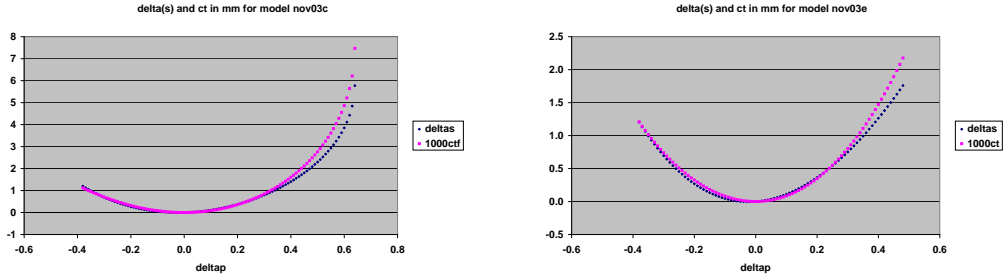


Figure 3: Variation of orbit length  $\delta s$  and flight time  $ct$  in mm for a cell with the relative momentum error  $\delta p/p$ , for sector dipoles on the left, for rectangular dipoles on the right. Note that the scales are different.

## 2.2 Flight Time Spread

Fig. 3 shows the variation of the flight times with the momentum error  $\delta p/p$  for a single lattice cell, and give the results for two different calculations. The TWISS command in MAD [2] provides those labelled  $\delta(s)$ , which is probably the difference in the path length between an off-momentum orbit and the reference or-

bit. Tracking with the TRACK command, starting on the off-momentum closed orbit, yields  $ct$ , which is probably the difference in flight time between the off-momentum and the reference particle, multiplied by the speed of light  $c$ . Both  $\delta(s)$  and  $ct$  vanish at  $\delta p/p = 0$ . In both magnet styles, the slopes of  $\delta(s)$  and  $ct$  are almost zero at  $\delta p/p = 0$ , and there is a quadratic variation of  $\delta(s)$  and  $ct$ . The spread in flight times is less than about 1 mm for  $-0.34 \leq \delta p/p \leq 0.32$  in the lattice with sector magnets, and for  $-0.34 \leq \delta p/p \leq 0.33$  in the lattice with rectangular magnets. The differences between  $\delta(s)$  and  $ct$  indicate that the MAD [2] calculation is not very accurate.

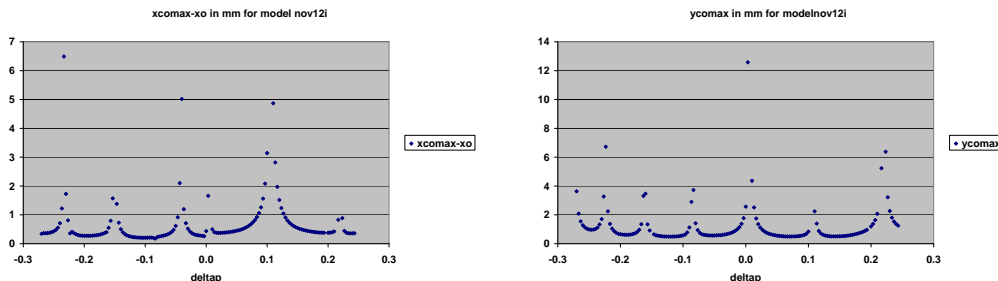


Figure 4: Maxima of the absolute values of the horizontal and vertical orbit offset  $x_{co}^{\max}$  and  $y_{co}^{\max}$  in mm due to the misalignment as a function of the relative momentum error  $\delta p/p$ . All 99 rectangular dipoles are displaced individually.

### 2.3 Misalignments

We were discouraged by the results of initial trials of random displacements of the dipoles with a standard deviation of 0.1 mm. Hence, we adopted a standard deviation of 0.03 mm, which we shall justify later. The distribution of the displacements is a Gaussian, truncated at 2.5 standard deviations. Fig. 4 shows the maxima of the absolute values of the horizontal and vertical orbit offset  $x_{co}^{\max}$  and  $y_{co}^{\max}$  due to the misalignment as a function of the relative momentum error  $\delta p/p$ . Here,  $y_{co}^{\max}$  is printed by MAD. We obtain  $x_{co}^{\max}$  from the value printed by MAD by subtracting the maximum absolute value of the horizontal orbit offset in the perfect machine, in order to remove the contribution of the dispersion  $D_x$  and  $\delta p/p$ . In Fig. 4 all 99 dipoles in the model ring are displaced individually. The spikes in  $x_{co}^{\max}$  and  $y_{co}^{\max}$  occur when the corresponding tunes  $Q_x$  or  $Q_y$  are close to an integer.

Fig. 5 shows  $x_{co}^{\max}$  and  $y_{co}^{\max}$  for the orbits of the reference particle at  $\delta p/p = 0$  due to the misalignment of all 99 individual dipoles for almost 300 samples. A sample is a complete ring with 99 displaced dipoles. All displacements are different. MAD does not find the closed orbit for one sample. Averaged over the

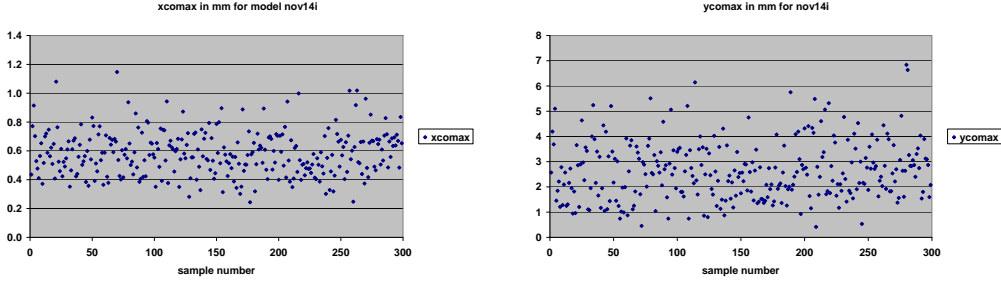


Figure 5: Maxima of the absolute values of the horizontal and vertical orbit offset  $x_{co}^{\max}$  and  $y_{co}^{\max}$  in mm for the reference particle at  $\delta p/p = 0$  due to the misalignment for almost 300 samples. All 99 rectangular dipoles are displaced individually.

remaining samples, we find  $x_{co}^{\max} = 0.58 \pm 0.15$  mm and  $y_{co}^{\max} = 2.6 \pm 1.2$  mm. The latter results is larger than the RMS beam radius, and invalidates our calculation of the vertical aperture. The nominal tunes at  $\delta p/p = 0$  are  $Q_x = 7.689$  and  $Q_y = 6.072$ . The proximity of  $Q_y$  to an integer probably explains the large orbit error  $y_{co}^{\max}$ .

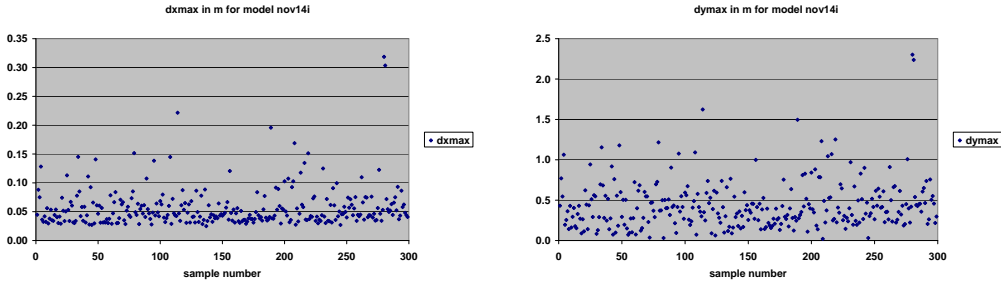


Figure 6: Maxima of the absolute values of the horizontal and vertical dispersion  $D_x$  and  $D_y$  in m for the reference particle at  $\delta p/p = 0$  due to the misalignment for almost 300 samples. All 99 rectangular dipoles are displaced individually.

Fig. 6 shows the maximum absolute values of horizontal dispersion  $D_x$  and  $D_y$  for the orbits of the reference particle at  $\delta p/p = 0$  due to the misalignment of all 99 individual dipoles for almost 300 samples. MAD does not find the closed orbit for one sample. Averaged over the remaining samples, we find  $D_x = 57 \pm 35$  mm and  $D_y = 436 \pm 303$  mm. The mean value of  $D_x$  is almost a factor of three larger than the design value. The mean value of  $D_y$  is unacceptable. The proximity of  $Q_y$  to an integer probably explains the large vertical dispersion  $D_y$ .

Figs. 7 and 8 show that the behaviour of the closed orbit and dispersion can be much improved by assuming that the dipole triplets are installed on a common girder with displacements that are much smaller than the displacements of the

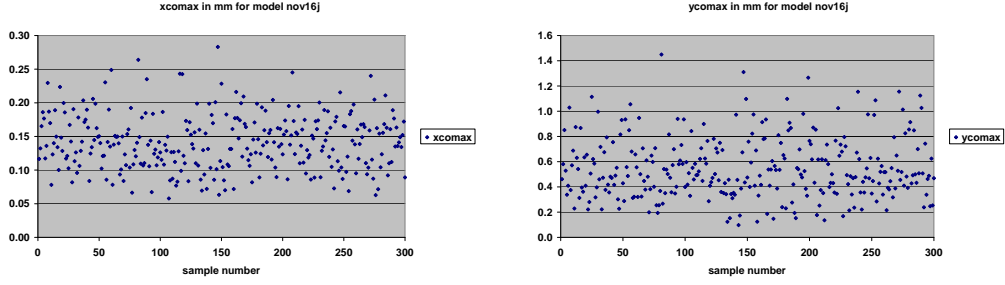


Figure 7: Maxima of the absolute values of the horizontal and vertical orbit offset  $x_{co}^{\max}$  and  $y_{co}^{\max}$  in mm for the reference particle at  $\delta p/p = 0$  due to the misalignment for 300 samples. The dipole triplets are installed on girders. The girders are displaced individually.

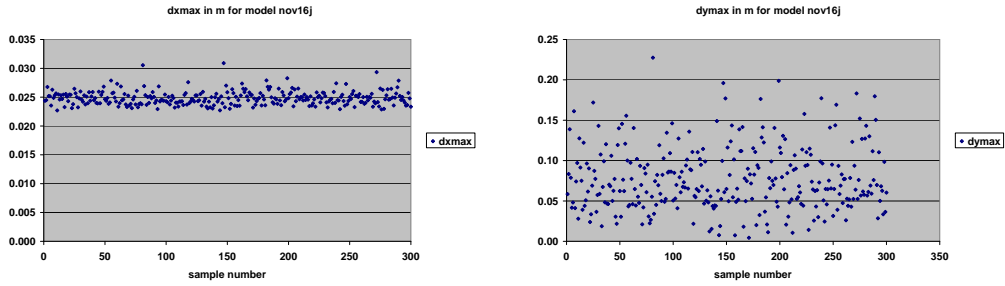


Figure 8: Maxima of the absolute values of the horizontal and vertical dispersion  $D_x$  and  $D_y$  in m for the reference particle at  $\delta p/p = 0$  due to the misalignment for 300 samples. The dipole triplets are installed on girders. The girders are displaced individually.

girders, which we still assume to have a standard deviation of 0.03 mm. MAD now finds the closed orbit in all 300 samples. Averaged over the samples, we find  $x_{co}^{\max} = 0.14 \pm 0.04$  mm and  $y_{co}^{\max} = 0.55 \pm 0.24$  mm,  $D_x = 25 \pm 1$  mm and  $D_y = 78 \pm 40$  mm. The horizontal dispersion  $D_x$  has small variations around the design value.

## 2.4 Aperture

MAD [2] provides easily the maxima of the absolute value of the orbit offset  $|x_c|$ , and of the  $\beta$ -functions  $\beta_x^{\max}$  and  $\beta_y^{\max}$  as functions of the relative momentum error  $\delta p/p$ . We use them to compute the half apertures  $A_x$  and  $A_y$ . To find the contribution of the betatron oscillations to the aperture, we assume that the electron beam has a normalised RMS emittance  $\varepsilon_n = 0.3$  mm, and allow for 3 RMS beam radii in the half aperture. We define  $\varepsilon_n$  as the product of the RMS beam radius  $\sigma$  and RMS momentum spread  $\Delta p/p_0$  in units of the muon rest momentum  $p_0$ .

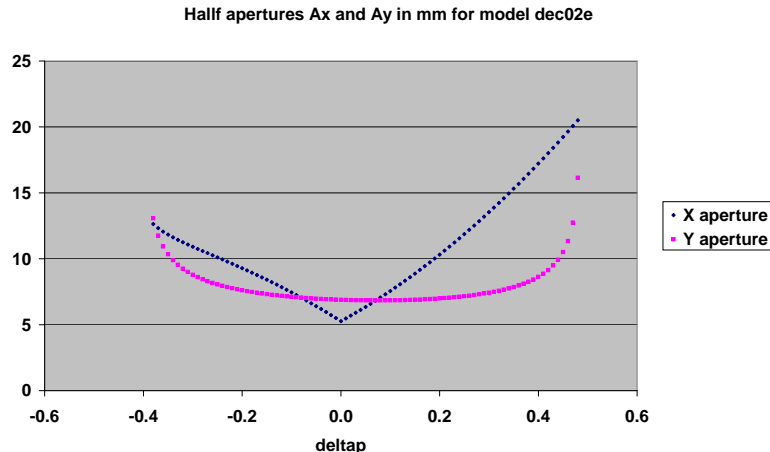


Figure 9: Horizontal and vertical half apertures in mm of a cell with rectangular dipoles as functions of the relative momentum error  $\delta p/p$

Our figure  $\varepsilon_n = 0.3$  mm is a factor three to five larger than that achieved in the LEP Injection Linac LIL at CERN [3]. In the horizontal plane, we add the betatron beam size to the orbit offset  $|x_c|$ . Fig. 9 shows the half apertures  $A_x$  and  $A_y$  thus obtained as functions of the relative momentum error  $\delta p/p$ . It may be seen that a vertical aperture radius  $A_y \approx 10.3$  mm and a horizontal aperture radius  $A_x \approx 15.3$  mm are needed for a momentum range  $-0.35 < \delta p/p < +0.35$  in the lattice with rectangular magnets. Our method of combining the maximum values of orbit offset  $|x_c|$  and  $\beta$ -functions  $\beta_x^{\max}$  and  $\beta_y^{\max}$  surely overestimates the vertical aperture  $A_y$  of the F magnets and the horizontal aperture  $A_x$  of the D magnets, and the magnetic field at the edge of the aperture in the D magnets.

## 2.5 Practical Lattice Considerations

The ratio of magnetic field and gradient  $B/G$  is the characteristic length, i.e. the lateral distance between the reference orbit and the radius where the magnetic field vanishes.

In the F magnets,  $B/G \approx -10$  mm is smaller than the horizontal aperture radius  $A_x$ . Hence, we assume that they are quadrupoles, displaced radially outwards by about 10 mm, rather than C or H shaped gradient dipoles. Allowing a few mm for closed orbit distortions, we take  $A_x = \pm 20$  mm and  $A_y = \pm 12$  mm for the horizontal and vertical aperture radius, respectively. With respect to the centre of the quadrupole, the horizontal aperture is at  $-30 \leq x \leq +10$  mm. Assuming that the hyperbolic pole face passes through the coordinates  $x = -30$  mm and  $y = 12$  mm, we find that the quadrupole bore radius is  $r_F \approx 26.8$  mm. Evaluating

the magnetic field at  $r_F$ , using the gradient listed in Tab. 1, yields about 0.35 T. The QL3 quadrupoles in the CTF3 test facility at CERN have gradient 11.2 T/m, bore radius 29 mm, quite similar to the F magnets, but are much longer with yoke length 0.2 m. Comparing their effective magnetic length 0.226 m to their overall length including coil overhangs 0.287 m shows that one coil overhang is about 30 mm, while the lattice design allows just about 20 mm for the coil overhangs of two neighbouring magnets. Adopting a coil design with just two layers would reduce the coil overhang by about 10 mm, and increase the transverse size of the quadrupole from 282 mm to about 302 mm. The cost of 14 QL3 quadrupoles was about 200 kCHF in early 2003.

In the D magnets,  $B/G \approx -35$  mm is larger than the horizontal aperture radius  $A_x$ . Hence, we assume that they are half quadrupoles with a neutral pole, radially outwards from the reference orbit. With respect to the neutral pole, the horizontal aperture is at  $-55 \leq x \leq -15$  mm. Assuming that the hyperbolic pole face passes through the coordinates  $x = -55$  mm and  $y = 12$  mm, we find that the quadrupole bore radius is  $r_D \approx 36.3$  mm. Evaluating the magnetic field at  $r_D$ , using the gradient listed in Tab. 1, yields about 0.23 T. The aperture and good field region extend well beyond the circle inscribed between the poles.

In order to achieve the alignment tolerance assumed above, with a standard deviation of about 0.03 mm, the following steps are recommended: (i) The triplets are installed on girders. The three magnets on a girder are aligned on a measuring table to much better precision than 0.03 mm. (ii) The model ring is installed on a solid block of reinforced concrete that is isolated from the rest of the building. (iii) The vertical alignment is done with usual levelling techniques. (iv) The horizontal alignment is done by measuring the distance of the girders from the centre of the model, either by invar rods or by laser interferometry. Invar wires pulling at the girders are not recommended. (v) The support of the vacuum chamber and air pressure is independent from that of magnets and girders.

### 3 Acceleration

Because of the vanishing slope of  $ct$  and  $\delta(s)$  at  $\delta p/p = 0$ , the FFAF ring has transition at the reference energy, and there are no buckets. Nevertheless, electrons are accelerated as can be seen in Fig. 10 and 11 for two accelerating voltages.

#### 3.1 Longitudinal Simulation in a Perfect Model

We launch particles below the unstable fixed point at  $ct = -50$  mm with  $-0.225 \leq p_t \leq -0.025$ , and track them for about 20 turns in the model ring. They are accelerated, and reach their maximum  $p_t$  at  $ct = -100$  mm, above the neighbouring

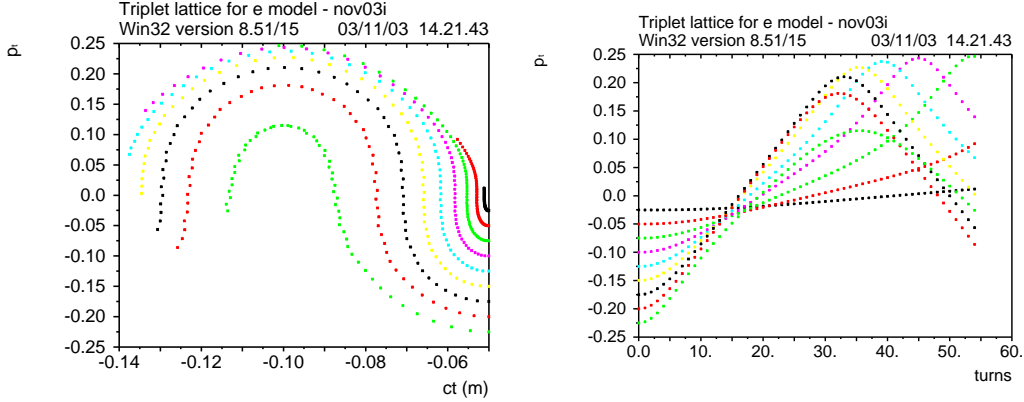


Figure 10: Acceleration in a ring consisting of 33 cells with rectangular dipoles and 0.66 MV peak circumferential RF voltage. Longitudinal phase space ( $ct, p_t$ ) is on the left, the relative momentum error  $p_t$  vs. "turns" is on the right. The abscissa "turns" is labelled in units of  $1/3$  of a turn.

stable fixed point. Particles launched at  $ct = -50$  mm with  $p_t \leq -0.25$  are either unstable or remain below  $p_t = 0$ , and are not shown. The initial and final momenta do not have equal magnitude and opposite sign. Electrons launched with lower  $p_t$  remain at lower  $p_t$ . The maximum acceleration is about 0.4 units of  $p_t$ , or from about 12 to about 18 MeV. More details are in the figure caption.

Fig. 11 demonstrates that the range of acceleration increases from about 0.4 to about 0.5 units of  $p_t$ , when the accelerating voltage on the RF cavities is increased from 20 to 50 kV.

### 3.2 Longitudinal Simulation in a Model with Alignment Errors

Fig. 12 shows the consequences of misalignments on the acceleration of particles. The triplets are installed on girders, which are displaced with 0.03 mm standard deviation, as in the first sample of the random displacements in Figs. 7 and 8. The peak circumferential accelerating voltage is 1.65 MV as in Fig. 11. Comparing Figs. 11 and 12 show very similar behaviour, apart from the two missing trajectories starting at  $\delta p/p = -0.15$  and  $\delta p/p = -0.3$ , and the factor of three in the number of observation points. However, it should be remembered that this simulation was done for individual particles, and not for bunches with finite emittances in all three degrees of freedom.

### 3.3 Practical RF Considerations

We assume that an RF cavity is installed in each of the 33 lattice cells. The total circumferential voltage, 0.66 MV, corresponds to  $V = 20$  kV accelerating voltage

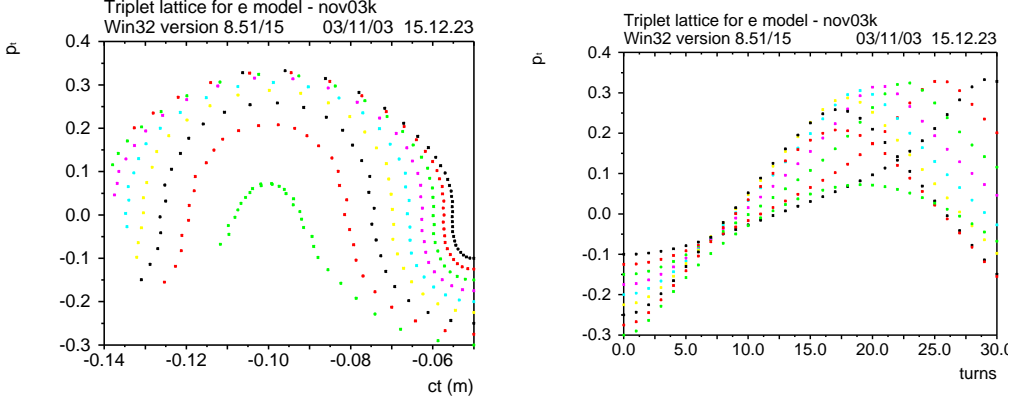


Figure 11: Acceleration in a ring consisting of 33 cells with rectangular dipoles and 1.65 MV peak circumferential RF voltage. Longitudinal phase space ( $ct, p_t$ ) is on the left, the relative momentum error  $p_t$  vs. "turns" is on the right. The abscissa "turns" is labelled in units of  $1/3$  of a turn.

in a cavity, or to 0.4 MV/m accelerating gradient. The peak voltage in the RF cavities  $U$  is larger than the accelerating voltage  $V$  by the reciprocal of the transit time factor which is  $2/\pi$  in a cavity of length  $\lambda_{\text{RF}}/2$ . We assume that the RF cavities have the shape of a pillbox and are made of copper with conductivity  $\sigma = 5.8 \times 10^7 \Omega^{-1}\text{m}^{-1}$ , neglect the beam ports, and follow [4]. Their intrinsic impedance is  $R/Q = 121 \Omega$ , their quality factor is  $Q = 17733$ . The RF power  $P$  needed in each RF cavity for  $V = 20$  kV is:

$$P = \frac{U^2}{2Q(R/Q)} = \frac{\pi^2}{8} \frac{V^2}{Q(R/Q)} = 230 \text{ W} \quad (1)$$

Typical buncher cavities in S band linacs are very similar to the RF cavities envisaged here. All RF cavities can be fed from a single CW power source, probably a travelling wave tube, with a single waveguide around the circumference of the ring, equipped with couplers that tap off the appropriate amount of RF power at every RF cavity. Whether to install 33 RF cavities in all the longer straight sections, or only every so often, is related to the optimisation of the RF system and the space needed for other equipment, e.g. injection and ejection kickers.

An idea about beam loading of the RF cavities is obtained by comparing the energy extracted by the beam  $W_e$  to the stored energy  $W_s$  in the cavity, which is given by:

$$W_s = \frac{U^2}{4\pi f_{\text{RF}}(R/Q)} \approx 0.216 \text{ mJ} \quad (2)$$

Here  $f_{\text{RF}} \approx 3$  GHz is the frequency of the RF system. With at most  $k = 33$  bunches in the beam, bunch population  $N$  and acceleration with  $n = 10$  turns, the

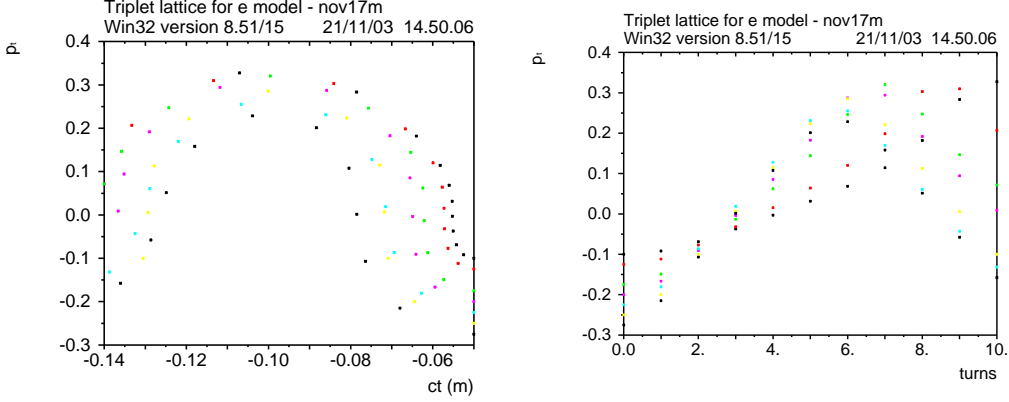


Figure 12: Acceleration in a ring consisting of 33 cells with rectangular dipoles and 1.65 MV peak circumferential RF voltage. The dipoles are installed on girders which are displaced with 0.03 mm standard deviation. Longitudinal phase space  $(ct, p_t)$  is on the left, the relative momentum error  $p_t$  vs. "turns" is on the right.

extracted energy  $W_e$  by all bunches and during all turns is

$$W_e = NVkne \quad (3)$$

Here,  $e$  is the electron charge. Taking  $W_e/W_s = 1$ , and solving for  $N$  yields an upper limit for the bunch population:

$$N \leq \frac{\pi V}{16kne f_{RF}(R/Q)} \approx 2 \times 10^8 \quad (4)$$

An accurate calculation of transient beam loading, taking into account the variation of phase and acceleration shown in Fig. 11 is beyond the scope of this note. The beam observation system in the model must work to the expected accuracy at about the bunch population in (4).

## 4 Conclusions

Parameters are derived and exhibited for the lattice and RF system of an electron model of a non-scaling FFAG ring, accelerating electrons from about 10 to 20 MeV. Spacings, magnet types and dimensions, and number of cells are presented. The model circumference is about 10 metres, and the magnet apertures are 10 mm  $\times$  20 mm. The tune variation with momentum is similar to that in a full machine, and would allow the study of resonance crossing. The variation of orbit length with momentum is less than 35 mm, and would allow the study of acceleration outside a bucket. A 100 mm straight section, in each of 33 cells, is adequately

long for an RF cavity operating at 3 GHz and is half an RF wavelength long. The accelerating voltage needed is calculated. Practical RF system design issues, e.g. RF power, and the limit on the bunch population due to beam loading are estimated.

Increasing the number of periods in the model ring from  $33 = 3 \times 11$  to  $36 = 2^2 \times 3^2$  would provide more flexibility in the choice of the number of RF cavities, etc. The nominal tunes at  $\delta p/p = 0$ ,  $Q_x = 8.388$  and  $Q_y = 6.624$ , would be well away from integral values, and the response of the vertical closed orbit to misalignments would be much improved.

Reducing the energy of the model by a factor of two, at constant circumference, and operating it between 5 and 10 MeV, would also reduce the magnetic fields by the same factor, and bring them into the range of permanent-magnet quadrupoles [5].

The simulation techniques presented can be applied not only to electron models, but also to FFAG rings accelerating muons.

## Acknowledgements

We should like to thank the participants in the recent FFAG workshop at BNL for stimulating discussions, and R. Corsini, G. Geschonke, W. Kalbreier, M. Mayoud, L. Rinolfi and T. Zickler at CERN for helpful advice.

## References

- [1] J.S. Berg, private communication.
- [2] H. Grote and F.C. Iselin, CERN SL/90-13 (AP) Rev.4 (1995).
- [3] J.P. Potier and L. Rinolfi, 6th European Particle Accelerator Conference (Stockholm, 1998), WEP17H, also CERN/PS 98-016(LP)(1998).
- [4] W. Schnell, in Handbook of Accelerator Physics and Engineering, eds. A.W. Chao and M. Tigner, 2nd printing (Singapore 2002) 526.
- [5] E. Keil, CERN-SL/2000-006 (AP) (2000).